

## RESEARCH ARTICLE

# Large-scale fabrication of core-shell triboelectric braided fibers and power textiles for energy harvesting and plantar pressure monitoring

Yingying Li<sup>1,2</sup> | Yihan Zhang<sup>2,3</sup> | Jia Yi<sup>1,2</sup> | Xiao Peng<sup>2,3</sup> | Renwei Cheng<sup>2,3</sup> |  
Chuan Ning<sup>2,3</sup> | Feifan Sheng<sup>1,2</sup> | Sen Wang<sup>1,2</sup> | Kai Dong<sup>2,3</sup>  |  
Zhong Lin Wang<sup>2,3,4</sup>

<sup>1</sup>Center on Nanoenergy Research, School of Physical Science and Technology, Guangxi University, Nanning, China

<sup>2</sup>CAS Center for Excellence in Nanoscience, Beijing Key Laboratory of Micro-Nano Energy and Sensor, Beijing Institute of Nanoenergy and Nanosystems, Chinese Academy of Sciences, Beijing, China

<sup>3</sup>School of Nanoscience and Technology, University of Chinese Academy of Sciences, Beijing, China

<sup>4</sup>School of Material Science and Engineering, Georgia Institute of Technology, Atlanta, Georgia, USA

## Correspondence

Kai Dong, CAS Center for Excellence in Nanoscience, Beijing Key Laboratory of Micro-Nano Energy and Sensor, Beijing Institute of Nanoenergy and Nanosystems, Chinese Academy of Sciences, Beijing 101400, China.

Email: dongkai@binn.cas.cn

Zhong Lin Wang, CAS Center for Excellence in Nanoscience, Beijing Key Laboratory of Micro-Nano Energy and Sensor, Beijing Institute of Nanoenergy and Nanosystems, Chinese Academy of Sciences, Beijing 101400, China.

Email: zlwang@gatech.edu

## Funding information

National Natural Science Foundation of China, Grant/Award Number: 22109012; Natural Science Foundation of Beijing Municipality, Grant/Award Number: 2212052; the National Key R & D Project from Minister of Science and Technology, Grant/Award Number: 2021YFA1201601; Fundamental Research Funds for the Central Universities, Grant/Award Number: E1E46805

## Abstract

Flexible and wearable energy harvesting devices and multifunctional sensors have been widely reported, but challenges in the large-scale manufacturing process still exist. This work reports a large-scale fabrication method of core-shell triboelectric braided fibers that exhibit stable structure and strong tensile strength, which can be further integrated into power textiles with different fabric structures, such as weaving and knitting, with the purpose of biomechanical energy harvesting or plantar pressure monitoring. The triboelectric braided fibers integrating on the knitting power textiles exhibit good pressure sensitivity and fatigue resistance, which is combined with traditional socks to measure the pressure distribution of the plantar in different positions. The weaving power textiles exhibit high electrical output, which can be used for biomechanical energy harvesting and can easily light up 116 commercial LEDs. This large-scale preparation approach provides more possibilities for power textiles applications in self-powered wearable electronics and human-computer interfacing.

## KEYWORDS

energy harvesting, large-scale fabrication, power textiles, pressure monitoring, triboelectric fibers

This is an open access article under the terms of the Creative Commons Attribution License, which permits use, distribution and reproduction in any medium, provided the original work is properly cited.

© 2022 The Authors. *EcoMat* published by The Hong Kong Polytechnic University and John Wiley & Sons Australia, Ltd.

## 1 | INTRODUCTION

With the advancement of society, smart wearable electronic devices become more and more popular because of their powerful functions and smart security.<sup>1,2</sup> Textiles are soft, comfortable, and breathable, providing more possibilities for the application of flexible wearable electronic devices.<sup>3–5</sup> Electronic textiles (e-textiles) have attracted great attention in academic circles.<sup>6,7</sup> As a flexible wearable electronic device, it can be integrated on various fabric substrates for health monitoring,<sup>8</sup> smart home care,<sup>9</sup> medical diagnosis,<sup>10</sup> and human motion detection.<sup>11,12</sup> However, wearable electronic devices often require external power sources and frequent charging to keep them running, which is not conducive to a wide range of applications.<sup>13,14</sup> Triboelectric nanogenerator (TENG) is a technology that uses the coupling effect of triboelectric and electrostatic induction to convert mechanical energy into electrical energy.<sup>15,16</sup> Textile TENG combines TENG with traditional clothing textile technology, which provides an alternative strategy for the power source of traditional flexible wearable electronic devices.<sup>17–19</sup> It can be used for energy harvesting, such as mechanical,<sup>20</sup> wind,<sup>21</sup> water drop,<sup>22</sup> and so forth. Meanwhile, textile TENGs also exhibit many advantages, such as diverse material options,<sup>23</sup> environmental friendliness,<sup>24</sup> low cost,<sup>25</sup> and so on.

In addition, textile TENGs can also be used as flexible sensors for human motion monitoring (walking, running, etc.),<sup>26,27</sup> respiratory monitoring,<sup>28</sup> sleeping monitoring,<sup>29</sup> and so on. Although textile TENGs have been widely used in the field of flexible sensing, it ignores the key issue of smart fabrics preparation process, which makes it limited in scale preparation and application to different degrees.<sup>30</sup> For example, most triboelectric fibers are usually prepared by coating a dielectric material on a conductive material.<sup>31,32</sup> The preparation process is complicated, costly, long preparation time, and inhomogeneous.<sup>33,34</sup> By directly coating conductive materials on the surface of traditional clothing, the air permeability and comfort of the smart fabrics will be reduced.<sup>35</sup> Moreover, as the washing time increases, the substance coated on the surface will gradually fall off.<sup>31</sup> All these problems seriously restrict the application of textile TENGs in wearable flexible devices. To solve these problems, several scholars have studied them and reported methods to prepare fiber-shaped TENGs on a large scale (e.g., infusing conductive materials into hollow dielectric materials, or using weaving and winding).<sup>19,26,27,34,36</sup> However, the prepared fibers do not meet the requirements of industrial textiles due to strength or process problems, or use vertical contact–separation mode, which limits the scope of application.

Here, we reported a large-scale method to fabricate core-shell triboelectric braided fibers. The triboelectric

braided fibers with uniform thickness and continuous length were prepared by braiding poly (vinylidene fluoride) (PVDF) yarns around silver-coated nylon yarns. The core-shell triboelectric braided fibers can be further expanded to power textiles based on different fabric forming techniques, such as weaving and knitting, to realize energy harvesting and self-powered sensing functions. The weaving power textiles with good stability, washability, and high output power density (1008  $\mu\text{W}/\text{m}^2$ ) can be used for energy harvesting. In addition, the knitting power textiles with high tensile strength and pressure sensitivity can be used to detect plantar pressure mapping under different postures of the human body, which shows the huge application potential of smart wearable devices in human motion.

## 2 | RESULTS AND DISCUSSION

The industrial manufacturing of fiber-shaped TENGs was one of the key problems for the extensive development of textile TENGs. To overcome the shortcomings of complex preparation process and inability to continuous production, it is necessary to select materials and optimize preparation process. Industrial PVDF yarn with stable performance and good abrasion resistance was selected as the dielectric material. Commercial silver-coated nylon yarn with low cost, easy to access, and scalable industrial production was used as the electrode. The core-shell triboelectric braided fibers are prepared by a high-speed rope braiding machine, as shown in Figure 1A. When the high-speed braiding machine works, as the disc rotates the PVDF yarns are divided into two groups, clockwise and counterclockwise, and cross-braided on the central conductive yarn. Figure S1A shows the action trajectory of the shell yarn (PVDF yarn) during the operation of the high-speed braiding machine. The structure of the core-shell triboelectric braided fibers is shown in Figure 1B. By cross-winding, the PVDF yarns can be wound more densely and uniformly on top of the central silver-plated nylon yarn. With the help of the top winding device, triboelectric braided fibers are wound continuously on the drum without length limitation, as shown in Figure 1C. Photograph of PVDF-Ag yarn of about 3 m in length, as shown in Figure S2. Figures 1D,E shows the cross-sectional scanning electron microscopy (SEM) image and the surface morphology SEM image of the triboelectric braided fibers consisting of eight axially wound yarns and one conductive yarn, respectively. The cross-sectional SEM image shows the silver-plated nylon yarn inside the circle marked by the red dashed line and the braided PVDF yarn outside, and the surface morphology SEM image shows that the PVDF yarn is wrapped very

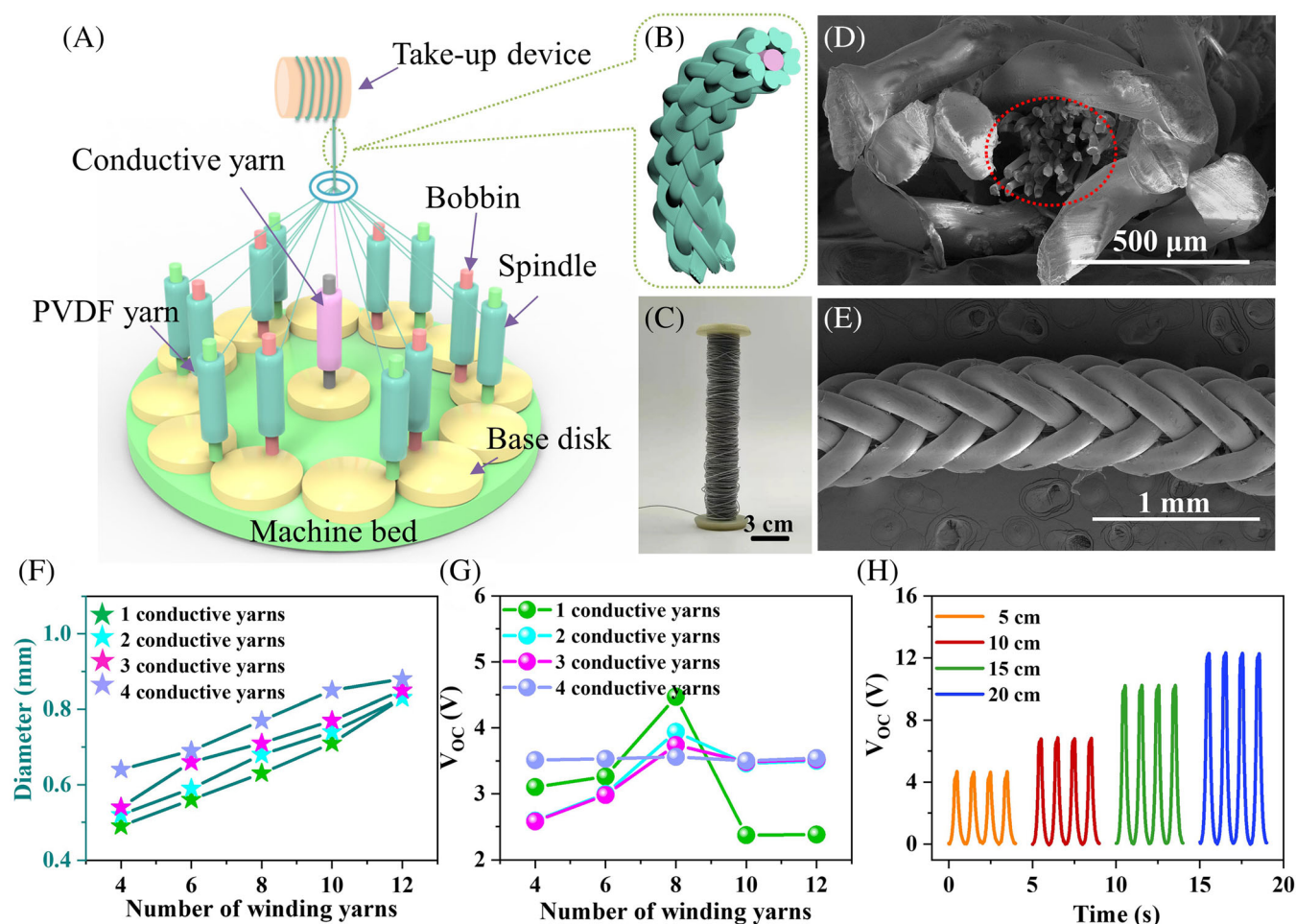


**FIGURE 1** Structure design and performance analysis of the core-shell triboelectric braided fibers. (A) Schematic diagram of high-speed rope braiding machine. (B) Structural diagram of the core-shell triboelectric braided fibers. (C) Photograph of the core-shell triboelectric braided fibers. (D) Cross-sectional scanning electron microscopy (SEM) image of the core-shell triboelectric braided fibers. (E) Surface morphology SEM image of the core-shell triboelectric braided fibers. (F) The diameter of the core-shell triboelectric braided fibers under different numbers of winding yarns and number of conductive yarns. (G) Open-circuit voltages ( $V_{OC}$ ) of the core-shell triboelectric braided fibers under different numbers of winding yarns and number of conductive yarns. (H)  $V_{OC}$  of the core-shell triboelectric braided fibers with eight axial winding yarns and one conductive yarn under different lengths

uniformly and densely, indicating that the core yarn is fully covered by the shell yarn. Figure S1B,C show the smooth surface of PVDF yarn and silver-plated nylon yarn, proving that the high-speed rope braiding machine does not damage the yarn surface. This method enables efficient and continuous preparation of regular triboelectric braided fibers.

To further investigate the performance of the core-shell triboelectric braided fibers, triboelectric braided fibers with different strands of silver-plated nylon yarn and PVDF yarn are prepared, as shown in Figure S3. When the number of PVDF yarn strands is four or six, the conductive yarn cannot be completely covered by the PVDF yarn, resulting in partial charge leakage and low electrical output. When the PVDF yarn is eight strands, with the increase of the number of central conductive

yarn, the PVDF yarn wrapping effect is getting worse (only one strand of conductive yarn wrapping is better), as shown in Figure S4A. When the number of PVDF yarns is increased to 10 or 12 strands, the non-uniformity of the shell surface and the inability of the conductive yarn to be tightly wrapped leads to a decrease in electrical output performance, as shown in Figures S4B,C and S5. The diameters of triboelectric braided fibers with different strand numbers are also investigated. The results show that the diameter (Figure 1F) and cross-sectional area (Figure S6A) of the triboelectric braided fibers increase with the increase of the number of winding yarns. This indicates that PVDF yarns are tightly wound with silver-plated nylon yarns. The electrical output performance of the triboelectric braided fibers is further investigated by testing the open-circuit voltage ( $V_{OC}$ ),

short-circuit current ( $I_{SC}$ ) and short-circuit charge transfer ( $Q_{SC}$ ) of the triboelectric braided fibers at different strand counts of PVDF yarns and silver-plated nylon yarns, as shown in Figure 1G, Figure S6B,C, respectively. The results show that the core-shell triboelectric braided fibers with eight axial winding yarns and one conductive yarn has the highest electrical output. Therefore, this

kind of core-shell triboelectric braided fibers with the diameter of 0.63 mm (Figure 1F) for fabricating power textiles. To better understand the mechanical properties of this core-shell triboelectric braided fibers, the stress-strain curves are tested as shown in Figure S7A, which has a strong tensile strength (158 MPa) but a low elongation at break (145%). The  $V_{OC}$  (Figures 1H and S8A),

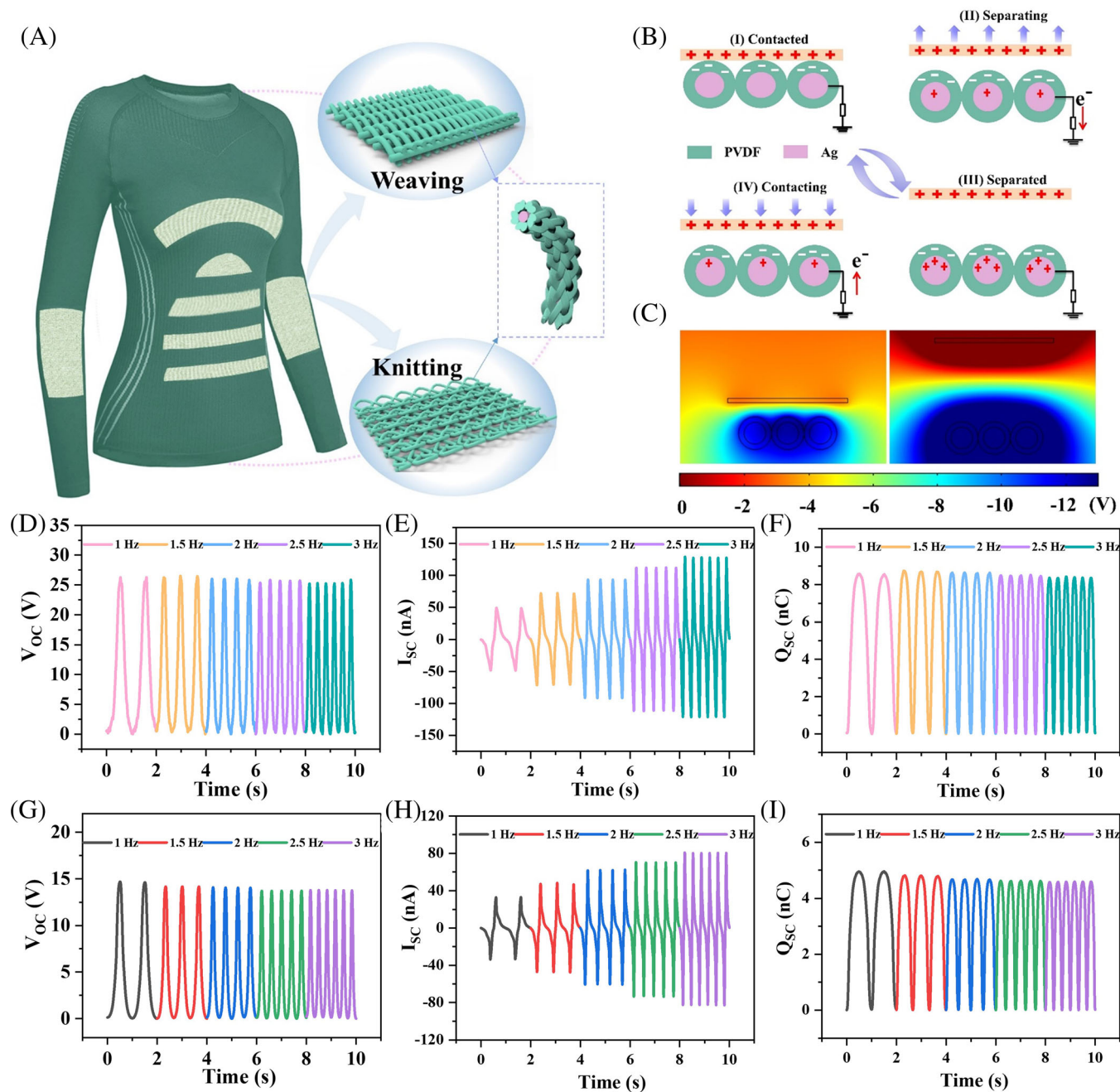


**FIGURE 2** Structural characteristic, operational principle, and output performance of the core-shell triboelectric braided fibers integrating on weaving and knitting power textiles. (A) Schematic illustration of different structures power textiles on clothing. It includes the structure of the core-shell triboelectric braided fibers, the weaving textiles, and the knitting power textiles. (B) Schematic diagram of operation principle of power textiles in contact-separation mode. (C) The electrical potential distribution is simulated by COMSOL software. (D)  $V_{OC}$ , (E)  $I_{SC}$ , and (F)  $Q_{SC}$  of the weaving power textiles under different loading frequencies (1–3 Hz). (G)  $V_{OC}$ , (H)  $I_{SC}$ , and (I)  $Q_{SC}$  of the knitting power textiles under different loading frequencies (1–3 Hz)

$I_{SC}$  (Figures S7B, S8B), and  $Q_{SC}$  (Figures S7C, S8C) of this triboelectric braided fibers at different lengths show that the electrical output increases with the increase of length (Supporting Note 1). It indicates that the triboelectric braided fibers can be applied to textile technology to manufacture large areas for energy harvesting and sensing.

The core-shell triboelectric braided fibers can be further integrated into power textiles with different fabric structures for biomechanical energy harvesting and self-powered sensing. Figure 2A shows the schematic diagram of the developed power textiles with different structures, which includes the weaving and the knitting power textiles. Weaving power textiles are made of interwoven warp and weft yarns while knitting power textiles are made of alternating loops. The operating principle of the core-shell triboelectric braided fibers and power textiles is briefly demonstrated in Figure 2B. It is a single-electrode working mode that involves the conjunction of contact electrification and electrostatic induction.<sup>15</sup> In the original state, when the free-moving object (material chosen opposite to the PVDF friction electrode, such as PMMA, skin, etc.) contacts the PVDF surface, the two contact surfaces will generate equivalent positive and negative electrostatic charges due to opposite polarities (Figure 2B, I).<sup>23</sup> As the two surfaces move away from each other, the potential of the electrode layer will rise, driving the flow of electrons to the ground and thus generating a current (Figure 2B, II). When the gap between the two electrically charged surfaces is large enough, a new equilibrium state will be established and electrons will stop moving (Figure 2B, III). When the free-moving object approaches to PVDF again, electrons flow from the ground to the electrode layer to achieve charge balance (Figure 2B, IV). When the free-moving object is in full contact with the PVDF again, the two surfaces are in equilibrium again. Almost no electrical output is observed at this time. This is the entire working cycle of the triboelectric braided fibers and its derived power textiles. To support the proposed mechanism of the electricity generating process, the electric potential between the PMMA film and the PVDF is simulated by using the COMSOL software (Figure 2C).

To characterize the output performance of the weaving and knitting power textiles, a measurement platform was established, as shown in Figure S9. The power textiles with an area of  $40 \times 45 \text{ mm}^2$  were fixed on an acrylic plate, another acrylic plate was attached to the vibrating surface of the linear motor. When the linear motor was working, the acrylic plate will contact the power textiles regularly.  $V_{OC}$ ,  $I_{SC}$  and  $Q_{SC}$  were measured in the frequency range of 1–3 Hz for weaving and knitting power textiles. The electrical output of the weaving

power textiles is  $V_{OC}$  of 26 V,  $Q_{SC}$  of 8.5 nC and  $I_{SC}$  (3 Hz) of 129 nA as shown in Figure 2D–F. The electrical output of the knitting power textiles is 14.6 V for  $V_{OC}$ , 4.9 nC for  $Q_{SC}$ , and 80.7 nA for  $I_{SC}$  (3 Hz) as shown in Figure 2G–I. The results show that the  $V_{OC}$  and  $Q_{SC}$  of power textiles are stable with increasing impact frequency, and the  $I_{SC}$  increases with increasing impact frequency. The electrical output of the weaving power textiles is higher than those of knitting power textiles, which is due to that the contact area of the weaving power textiles being larger than that of the knitting power textiles under the same conditions. Therefore, the weaving power textiles can be used for energy harvesting. In addition, the knitting power textiles have excellent stretchability due to its alternating coil structure and can be used as a fabric sensor. In the following, the energy harvesting performance of weaving power textiles and the self-powered sensing performance of knitting power textiles are discussed separately.

To further explore the energy harvesting performance of the weaving power textiles, its electrical output performance was tested (Figure S10A). Figure 3A shows the variation of current and power density of the weaving power textiles with different external load resistance. The output power density is measured by externally connecting different loads from 10 k $\Omega$  to 50 G $\Omega$  under the frequency of 1 Hz. When the loading resistance is below 1 G $\Omega$ , there is no significant change in the output current. The output current decreases when the load resistance increases from 1 to 50 G $\Omega$ . At a load resistance of 3 G $\Omega$ , the maximum output power density is 1008  $\mu\text{W}/\text{m}^2$  (Figure 3A). In addition, as shown in Figure 3B, the stability of the weaving power textiles is tested by continuously tapping it about 6000 cycles with a stable  $V_{OC}$  around 24 V. The insets exhibit the detailed  $V_{OC}$  for the early 10 cycles and the last 10 cycles, respectively. It shows that the weaving power textiles have well stability. The electricity generated from the weaving power textiles can be further stored in commercial capacitors. The alternating current (AC) output of the weaving power textiles can be converted to direct current (DC) output through the bridge circuit. The charging process of the weaving power textiles for different capacitors (0.33, 0.47, 1, 2.2, 4.7, 6.8, and 220  $\mu\text{F}$ ) is shown in Figure 3C. The charging rate decreases with increasing capacitance. Washability is very important for the long-term reuse of power textiles. In this study, the domestic washing environment is developed using a magnetic stirrer, as shown in Figure S10B. The weaving power textiles are stirred in a beaker with a magnetic stirrer with water for 20 min at a time. To test the washability of the weaving power textiles, we tested the output voltage under 15 washes, as shown in Figure 3D. It can be found that only a slight

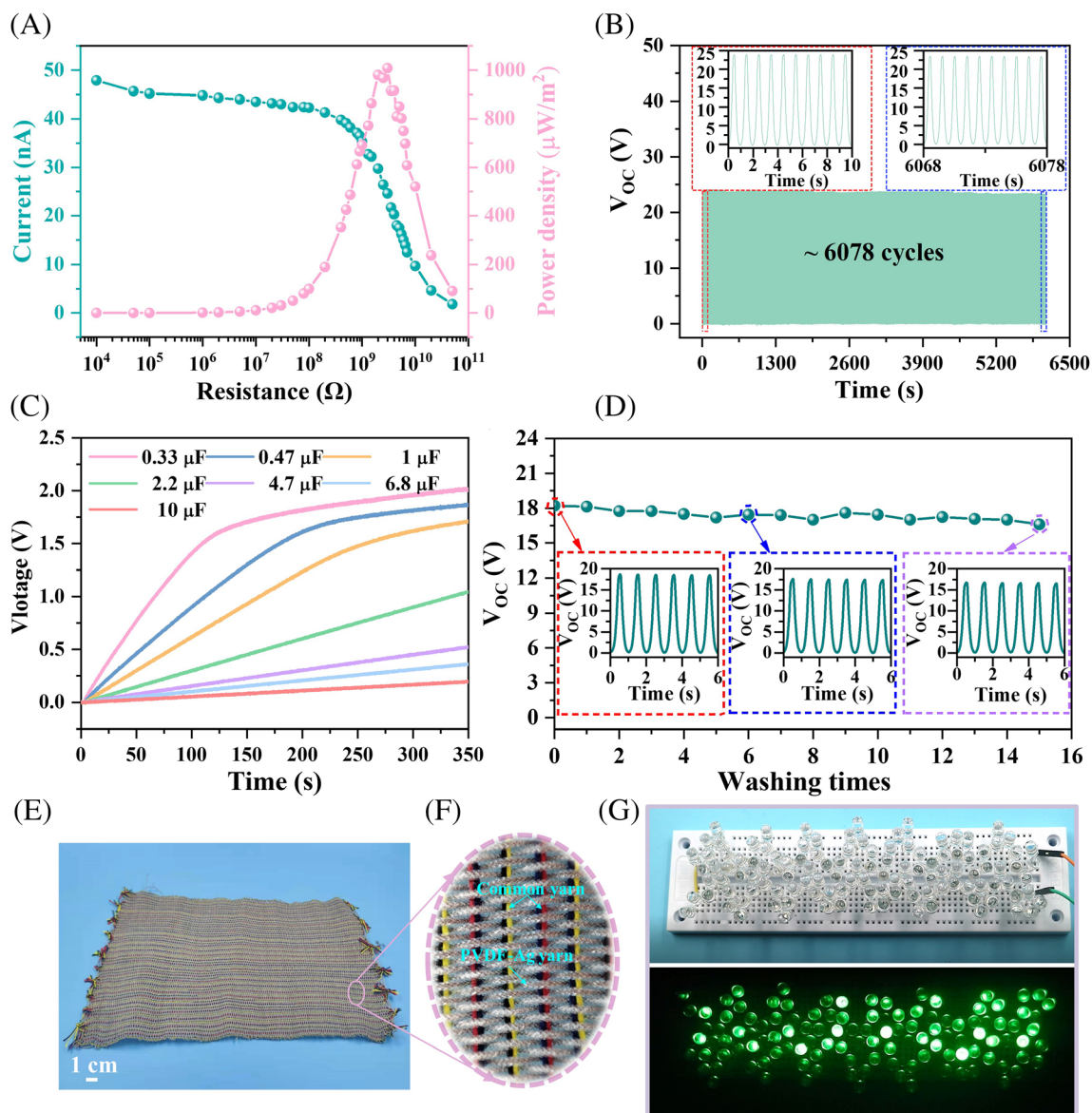


**FIGURE 3** Energy harvesting performance of the weaving power textiles. (A) The variation of current and power density of the weaving power textiles with different external load resistance. (B) The stability test of the weaving power textiles. The insets exhibit the  $V_{OC}$  of the early 10 cycles and the last 10 cycles. (C) Charging curves of weaving power textiles under different capacitance capacities. (D) The  $V_{OC}$  of the weaving power textiles at different washing times. The insets show the  $V_{OC}$  of the unwashed, the sixth washed and the 15th washed, respectively. (E) Photographs of large-area weaving power textiles. (F) The partially enlarged view of the weaving power textiles, which shows its two components including common yarn warp yarn and PVDF-Ag yarn weft yarn. (G) Photograph showing the weaving power textiles powering 116 LEDs in series

decrease in the output voltage is observed throughout the washing tests. This means that weaving power textiles is the potential for a wide range of applications in everyday life as far as good washability is concerned. The core-shell triboelectric braided fibers and common yarns are used to make large-area energy harvesting weaving power textiles in small braiding tools (Figure 3E). Figure 3F shows a partial enlargement of the weaving power textiles, which consists of two parts: common yarn warp yarns and the core-shell triboelectric braided fibers

weft yarns. As shown in Figure S10C, the weaving power textiles can sustain various kinds of complex mechanical deformations, including folding and crimping. Figure 3G shows that the weaving power textiles can power up 116 LEDs (Movie S1). These demonstrations show that the energy harvesting by the weaving power textiles can not only be stored in energy storage devices but can also be used to drive wearable devices.

The pressure-sensitive properties of knitting power textiles were investigated by relating the electrical output

of the fabric to the applied pressure. As shown in Figure 4A,  $V_{OC}$  increases with increasing applied pressure. The maximum  $V_{OC}$  generated by the knitting power textiles is 11 V at 144 Pa under tapping force. When the applied pressure approaches 19 kPa, the  $V_{OC}$  is 18.5 V. As shown in Figure 4B, the output voltage signal is uniform and repeatable when the applied pressure is constant. At a smaller loading force, the knitted stitches (Figure S11) do not make sufficient contact with each other and the output is smaller. As the loading force increases, the contact area between the knitted stitches increases, thus increasing the electrical output of the knitting power textiles. Figure 4A divides the curve into two pressure regions. In the low-pressure areas (0–3.7 kPa), the pressure sensitivity of knitting structure power textiles is  $0.84 \text{ V kPa}^{-1}$ . In the high-pressure areas ( $>3.7 \text{ kPa}$ ), the pressure sensitivity is  $0.27 \text{ V kPa}^{-1}$ . This phenomenon is

because the increment of real contact area in response to pressure in low-pressure areas is much larger than that in high-pressure areas. Therefore, the knitting power textiles exhibit a more sensitive response in the low-pressure region ( $<3.7 \text{ kPa}$ ). The electrical output with pressure change for weaving power textiles (Figure S12), and the comparison revealed that the sensing characteristics of knitting power textiles are better in the high pressure region. In addition, the alternating loop structure of the knitting power textiles can also exhibit various complex mechanical deformations as shown in Figure 4C. Figure 4C (I–IV) shows the original state, the crimping state, the XY direction stretching state and the X direction stretching state of the knitting power textiles, respectively. To investigate the tensile fatigue of the knitting power textiles, stress–strain cyclic curves are tested as shown in Figure 4D. The results show that the knitting

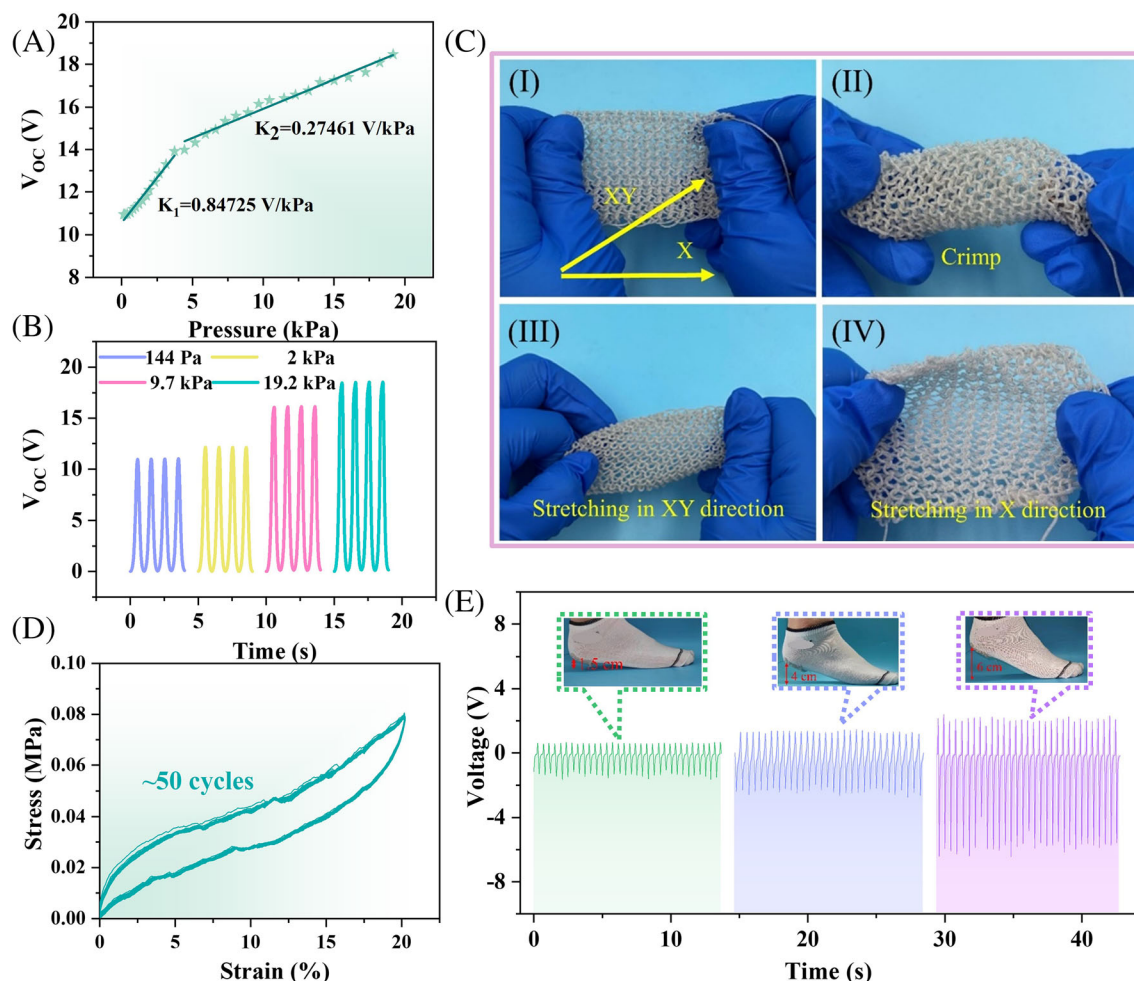


**FIGURE 4** Sensing features and demonstration of the knitting power textiles. (A) The output voltage of the knitting power textiles as a function of loading pressure variations. (B) The output voltage of the knitting power textiles under different pressures. (C) Photographs of the knitting power textiles under various mechanical deformations, including stretching and crimping. (D) Stress–strain curves of the knitting power textiles being stretched and released for 50 cycles. (E) The peak value of voltage of knitting power textiles under different heights of the heel, including 1.5, 4, and 6 cm. The insets are schematics of the knitting power textiles on the sock

power textiles exhibit well fatigue resistance after 50 stretching cycles. The knitting power textiles have good flexibility. The knitting power textiles were stretched to different degrees, and the relationship of electrical output with pressure variation and the stability of stretch sensitivity were tested. As shown in Figure S13, the results show that the sensing stability of the knitting power textiles is good. A self-powered human motion detector has been developed based on the excellent flexibility and sensitivity of knitting power textiles. The knitting power textiles are sewn onto the heel of a sock because the heel maximizes contact with the ground as shown in Figure S14. As shown in Figure 4E, the periodic contact interval between the heel and the ground generates periodic electrical signals when the human body moves. As the heel rises to different heights and then descends, the pressure on knitting power

textiles increases with height and the peak output voltage increases. According to these electrical signals, we can understand the movement behaviors of the human body and record the number of steps. The above studies show that knitting power textiles can be used for human movement monitoring and have potential applications in the field of exercise and health.

Plantar pressure distribution is widely recognized in human disease diagnosis, biomechanics, and gait analysis.<sup>37</sup> For example, the diagnosis of plantar pressure can predict diabetic foot ulcers<sup>38</sup> and predict diseases affecting the foot and ankle.<sup>39</sup> Here, we developed a smart sock that combines knitting power textiles with conventional socks to produce a smart sock that can be used to detect the distribution of plantar pressure. Figure 5A shows the plantar pressure mapping system. The whole plantar

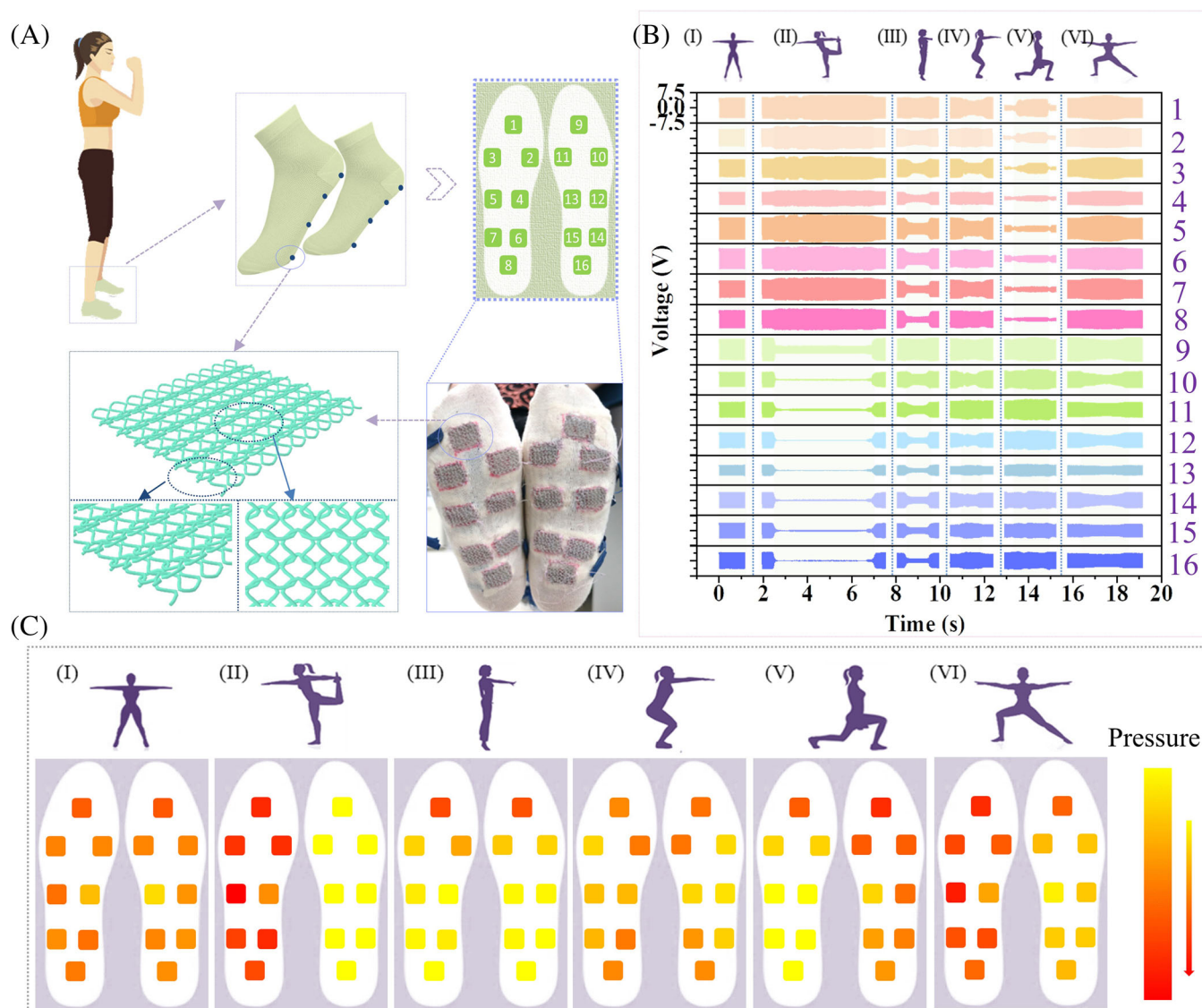


FIGURE 5 A plantar pressure mapping system for different poses. (A) Schematic plantar pressure mapping system. (B) Voltage output signals of the six typical poses. (C) Plantar pressure mapping distributions were recorded for six typical poses

pressure mapping system is composed of three main parts: intelligent socks, signal processing circuit and computer-based on Labview program. As shown in Figure S15A, the smart sock integrates 16 knitting power textiles, each knitting power textile as an independent one sensing sensor unit (area of  $20 \times 25 \text{ mm}^2$ ), and as mutually independent channels from each other. The 16 sensing sensor units are defined as corresponding numbers and are located in the corresponding locations of the forefoot (1 and 9), metatarsals (2, 3, 10, and 11), midfoot (4–7 and 12–15) and heel (8 and 16) areas. Figure S15B shows the physical diagram of the smart sock. When a person puts on smart socks and stands, the output different voltages due to different pressures applied of the sensor at the bottom of the sock. The voltage signals will be converted into digital signals through the analog-to-digital (A/D) converter, which in turn will trigger the multi-control unit. After signal conversion processing, the real-time results of plantar pressure can be displayed in the designed program. As expected, in the standing posture, the pressures on both feet are equal, with the lowest pressure in the arch region (sensors 4 and 13) and an even distribution of pressure in the remaining positions. The output voltage values and plantar pressure mapping of the 16 single sensing sensor units at the bottom of the sock in the standing posture are shown in Figure 5B (I) and Figure 5C (I), respectively (Movie S2).

In addition, the volunteers practiced eight different yoga postures, standing on one foot, stand-on-toe, squat, forward lunge, side lunge, step, turn and twist. The results suggest several characteristic patterns of the plantar pressure distribution along with the changes in yoga postures. When standing on one left foot, the left foot bears most of the weight of the body, and the plantar pressure value is much higher than that of the right foot. For the standing-on-toes position, plantar pressure is concentrated in the forefoot area (sensors 1 and 9), with decreased plantar pressure in the metatarsal, mid-foot and heel regions. In the squat posture, the pressure distribution of both feet is uniform, the pressure value of the outside of both feet decreases, and the pressure value of the inside of both feet increases. In the forward lunge posture, the body's center of gravity moves forward and the pressure on the right foot increases, with the greatest pressure on the front of the right foot. At this time, the front of the left foot is in contact with the ground but with less pressure, and the rest of the left foot is not in contact with the ground. In the side lunge posture, shift your weight to the left and increase pressure on your left foot. The pressure on the right foot decreases, the pressure on the front of the right foot changes little, the pressure on the heel and arch area is the lowest. The output

voltage values and plantar pressure mapping of the five postures as shown in Figure 5B (II–VI) and Figure 5C (II–VI), respectively (Movie S2). Three other postures: step, turn and twist. Their output voltage values and plantar pressures are shown in Figure S15C (I–III) and D (I–III), respectively. In the step position, when the right foot is raised, the center of gravity shifts to the left foot. At this time, the plantar pressure value of the left foot is much higher than that of the right foot. Alternating feet, the center of gravity also alternates. For the turn posture, the pressure on the outside of the feet changes with the turning posture. When twisting the posture, the center of gravity changes in a circle with the body twisting the waist, and the plantar pressure also changes in a circle with the center of gravity. The pressure on the bottom of the foot in all three positions also varies with the posture. In conclusion, smart socks are sensitive and can easily detect the mapping of the foot pressure in different postures of the body, providing interesting application scenarios in wearable smart sports.

### 3 | CONCLUSION

In summary, the preparation method of the core-shell triboelectric braided fibers is simple, continuous, homogeneous and suitable for large-scale industrial production. The core-shell triboelectric braided fibers are fabricated with eight axially wound yarns (PVDF yarn) as the shell and one conductive yarn (silver-plated nylon yarn) as the core. Moreover, the core-shell triboelectric braided fibers are further prepared to power textiles with weaving and knitting structures that are washable, deformable, breathable, and comfortable. The weaving power textiles exhibit high electrical output ( $V_{OC}$  is 26 V,  $Q_{SC}$  is 8.5 nC and  $I_{SC}$  is 129 nA (3 Hz)), which can light up about 116 LEDs. The knitting power textiles exhibit stable tensile strength (approximately 50 stretch cycles), mechanical deformations, and high sensitivity. In addition, smart socks with the knitting power textiles as the sensing units are used for plantar pressure mapping of different human body postures, which show broad prospects in wearable smart textiles.

#### 3.1 | Experimental section

##### 3.1.1 | Materials

The commercial silver-coated nylon yarn was used for the conductive material, the nontoxic, harmless, stable performance and not easy to wear PVDF yarn were selected as the dielectric material. Socks are commercial cotton socks.

### 3.1.2 | The fabrication of the core-shell triboelectric braided fibers

Commercial silver-plated nylon yarn and commercial PVDF yarn were chosen as the conductive material and the dielectric material, respectively. The core-shell triboelectric braided fibers were fabricated by braiding on a high-speed rope braiding machine (Figure 1A). The central conductive yarn was wound on a fixed bobbin and fed through a tension device. The PVDF yarn was wound on the bobbin and secured to the outside yarn disc. When working, the outer yarn disc is divided into counterclockwise rotation and clockwise rotation. In the working process, the reciprocating movement from one disk to another was beneficial to the PVDF yarns winding on the conductive yarn to form the core-shell triboelectric braided fibers. The continuous supply of yarn was achieved by the rotation of the spool on the spindles. The number of spindles for winding the yarn depends on the number of feeding spindles. The number of conductive yarns were selected 1, 2, 3, and 4 strands, respectively. The number of winding yarns (PVDF) were selected in 4, 6, 8, 10, and 12 strands, respectively. The optical images of the core-shell triboelectric braided fibers were shown in Figure S3.

### 3.1.3 | Fabrication of weaving and knitting power textiles

In this work, the core-shell triboelectric braided fibers were used to fabricate power textiles with two structures: weaving and knitting, respectively. Although two structures were made by hand, the manufacturing technique was matured in the textile field and suitable for large-scale industrial production. The specific production method of weaving power textiles was as follows: First, selected common yarns and the core-shell triboelectric braided fibers as the warp yarns and weft yarns of structure weaving power textiles, respectively. The weft yarns were interwoven with the warp yarns to fabricate the weaving power textiles (Figure 2A). The air permeability could be adjusted by changing the density of the warp and weft during the weaving process. The knitting power textiles were mainly weft-knitting double-reverse texture (Figure 2A). It consists of front knitted loops and back knitted loops of loops alternating with each other in the horizontal (course) or vertical (wale). The knitting power textiles were relatively thick and exhibited vertical and horizontal elasticity.

### 3.1.4 | Washing test

Added tap water and magnetic stirring rod into the beaker, put into power textiles directly into the beaker without any packing. Place the fabricated beaker on a magnetic mixer to mimic the roller rotation of the household washing machine. The spinning speed of the magnetic agitator was set at 600 rpm, the whole washing process lasted for 20 min. The power textiles were then rapidly dried in an oven at 60°C. This work has been washed 15 times.

### 3.1.5 | Characterization and measurement

To characterize the electrical output performances of the core-shell triboelectric braided fibers and weaving and knitting power textiles, we use a linear motor to provide periodic contact-separation motion. The contact area is chosen as 50 mm and  $40 \times 45 \text{ mm}^2$ , respectively, the tapping force is applied as 10 N, and the maximum movement distance is set as 20 mm. The surface morphology of the silver-coated nylon yarns, PVDF yarn and the core-shell triboelectric braided fibers, respectively and the cross-sectional of the core-shell triboelectric braided fibers were characterized by field emission scanning electron microscope (Nova Nano SEM 450). For the measurement of the electrical output capability of the weaving and knitting power textiles, external forces were applied by a commercial linear mechanical motor. The  $V_{OC}$ ,  $I_{SC}$ , and  $Q_{SC}$  were measured by a Keithley 6514 electrometer.

### ACKNOWLEDGMENTS

The authors are grateful for the support received from the National Key R & D Project from Minister of Science and Technology (2021YFA1201601), National Natural Science Foundation of China (Grant No. 22109012), the Beijing Municipal Natural Science Foundation (Grant No. 2212052), and the Fundamental Research Funds for the Central Universities (Grant No. E1E46805).

### AUTHOR CONTRIBUTIONS

Kai Dong and Zhong Lin Wang proposed and supervised the project. Yingying Li participated in all aspects of this work from device fabrication to characterization and data processing. Yihan Zhang participated in capturing videos of equipment applications. Jia Yi and Feifan Sheng helped design the plantar pressure mapping system. Renwei Cheng and Chuan Ning were involved in device fabrication. Xiao Peng and Sen Wang assisted in analyzing the

data. All authors discussed the results and commented on the article.

## CONFLICT OF INTEREST

The authors declare no conflict of interest.

## ORCID

Kai Dong  <https://orcid.org/0000-0001-6314-1546>

## REFERENCES

- Cima MJ. Next-generation wearable electronics. *Nat Biotechnol.* 2014;32(7):642-643.
- Zhu Z, Tolar J, McAlpine MC, et al. 3D printed functional and biological materials on moving freeform surfaces. *Adv Mater.* 2018;30(23):e1707495.
- Di J, Li R, Li Q, et al. Carbon-nanotube fibers for wearable devices and smart textiles. *Adv Mater.* 2016;28(47):10529-10538.
- Zeng W, Shu L, Li Q, Chen S, Wang F, Tao XM. Fiber-based wearable electronics: a review of materials, fabrication, devices, and applications. *Adv Mater.* 2014;26(31):5310-5336.
- Weng W, Chen P, He S, Sun X, Peng H. Smart electronic textiles. *Angew Chem Int Ed Engl.* 2016;55(21):6140-6169.
- Fakharuddin A, Mohd Yusoff ARB, Vasilopoulou M, et al. Fiber-shaped electronic devices. *Adv Energy Mater.* 2021;11(34):2101443.
- Hatamvand M, Ahmed I, Zhan Y, et al. Recent advances in fiber-shaped and planar-shaped textile solar cells. *Nano Energy.* 2020;71:104609.
- Wang Y, Zhu M, Wei X, Yu J, Li Z, Ding B. A dual-mode electronic skin textile for pressure and temperature sensing. *Chem Eng J.* 2021;425:130599.
- Xu K, Wang X, Wei W, Song H, Mao B. Toward software defined smart home. *IEEE Commun Mag.* 2016;54(5):116-122.
- Kim J, Campbell AS, de Avila BE, Wang J. Wearable biosensors for healthcare monitoring. *Nat Biotechnol.* 2019;37(4):389-406.
- Praveen S, Santhoshkumar P, Joe YC, Senthil C, Lee CW. 3D-printed architecture of Li-ion batteries and its applications to smart wearable electronic devices. *Appl Mater Today.* 2020;20:100688.
- Wang Q, Peng X, Zu Y, Jiang L, Dong K. Scalable and washable 3D warp-knitted spacer power fabrics for energy harvesting and pressure sensing. *J Phys D Appl Phys.* 2021;54(42):424006.
- Dong K, Peng X, Wang ZL. Fiber/fabric-based piezoelectric and triboelectric nanogenerators for flexible/stretchable and wearable electronics and artificial intelligence. *Adv Mater.* 2020;32(5):e1902549.
- Shao J, Jiang T, Wang ZL. Theoretical foundations of triboelectric nanogenerators (TENGs). *Sci China Technol Sci.* 2020;63(7):1087-1109.
- Fan F-R, Tian Z-Q, Wang ZL. Flexible triboelectric generator. *Nano Energy.* 2012;1(2):328-334.
- Wang ZL, Chen J, Lin L. Progress in triboelectric nanogenerators as a new energy technology and self-powered sensors. *Energy Environ Sci.* 2015;8(8):2250-2282.
- Cheng R, Dong K, Wang ZL, et al. High output direct-current power fabrics based on the air breakdown effect. *Energy Environ Sci.* 2021;14(4):2460-2471.
- Dong K, Wang ZL. Self-charging power textiles integrating energy harvesting triboelectric nanogenerators with energy storage batteries/supercapacitors. *J Semicond.* 2021;38(10):101601.
- Dong S, Xu F, Sheng Y, Guo Z, Pu X, Liu Y. Seamlessly knitted stretchable comfortable textile triboelectric nanogenerators for E-textile power sources. *Nano Energy.* 2020;78:105327.
- Kwak SS, Yoon H-J, Kim S-W. Textile-based triboelectric nanogenerators for self-powered wearable electronics. *Adv Funct Mater.* 2019;29(2):1804533.
- Ye C, Dong K, Wang ZL, et al. A triboelectric-electromagnetic hybrid nanogenerator with broadband working range for wind energy harvesting and a self-powered wind speed sensor. *ACS Energy Lett.* 2021;6(4):1443-1452.
- Jiang C, Li X, Ying Y, Ping J. A multifunctional TENG yarn integrated into agrotexile for building intelligent agriculture. *Nano Energy.* 2020;74:104863.
- Wang ZL. Triboelectric nanogenerators as new energy technology and self-powered sensors—principles, problems and perspectives. *Faraday Discuss.* 2014;176:447-458.
- Xu W, Huang L-B, Wong M-C, Chen L, Bai G, Hao J. Environmentally friendly hydrogel-based triboelectric nanogenerators for versatile energy harvesting and self-powered sensors. *Adv Energy Mater.* 2017;7(1):1601529.
- Wang W, Zhai J, Wang ZL, et al. Large-scale fabrication of robust textile triboelectric nanogenerators. *Nano Energy.* 2020;71:104605.
- Dong K, Wang J, Wang ZL, et al. Shape adaptable and highly resilient 3D braided triboelectric nanogenerators as e-textiles for power and sensing. *Nat Commun.* 2020;11(1):1-11.
- Gao Y, Guan X, Yang Y, et al. Scalable core-spun coating yarn-based triboelectric nanogenerators with hierarchical structure for wearable energy harvesting and sensing via continuous manufacturing. *Nano Energy.* 2022;91:106672.
- Peng X, Wu Z, Wang ZL, et al. All-nanofiber self-powered skin-interfaced real-time respiratory monitoring system for obstructive sleep apnea-hypopnea syndrome diagnosing. *Adv Funct Mater.* 2021;31(34):2103559.
- Lin Z, Yang J, Yang J, et al. Large-scale and washable smart textiles based on triboelectric nanogenerator arrays for self-powered sleeping monitoring. *Adv Funct Mater.* 2018;28(1):1704112.
- Dong K, Hu Y, Yang J, Kim S-W, Hu W, Wang ZL. Smart textile triboelectric nanogenerators: current status and perspectives. *MRS Bull.* 2021;46(6):512-521.
- Ning C, Dong K, Wang ZL, et al. Flexible and stretchable fiber-shaped triboelectric nanogenerators for biomechanical monitoring and human-interactive sensing. *Adv Funct Mater.* 2020;31(4):2006679.
- He E, Gu B, Zhang W, et al. 3D angle-interlock woven structural wearable triboelectric nanogenerator fabricated with silicone rubber coated graphene oxide/cotton composite yarn. *Compos Part B: Eng.* 2020;200:108244.
- Karim N, Carr C, Novoselov KS, et al. Scalable production of graphene-based wearable E-textiles. *ACS Nano.* 2017;11(12):12266-12275.

34. Jing T, Xu B, Yang Y. Organogel electrode based continuous fiber with large-scale production for stretchable triboelectric nanogenerator textiles. *Nano Energy*. 2021;84:105867.
35. Feng PY, Mi HY, Liu Y, et al. Enhancing the performance of fabric-based triboelectric nanogenerators by structural and chemical modification. *ACS Appl Mater Interfaces*. 2021;13(14):16916-16927.
36. Yu A, Hu W, Wang ZL, et al. Core-shell-yarn-based triboelectric nanogenerator textiles as power cloths. *ACS Nano*. 2017;11(12):12764-12771.
37. Nie B, Liu J, Chen X, et al. Textile-based wireless pressure sensor array for human-interactive sensing. *Adv Funct Mater*. 2019;29(22):1808786.
38. Stess RM, Jensen SR, Mirmiran R. The role of dynamic plantar pressures in diabetic foot ulcers. *Diabetes Care*. 1997;20(5):855-858.
39. Schuh R, Trnka HJ, Sabo A, Reichel M, Kristen KH. Biomechanics of postoperative shoes: plantar pressure

distribution, wearing characteristics and design criteria: a preliminary study. *Arch Orthop Trauma Surg*. 2011;131(2):197-203.

## SUPPORTING INFORMATION

Additional supporting information may be found in the online version of the article at the publisher's website.

**How to cite this article:** Li Y, Zhang Y, Yi J, et al. Large-scale fabrication of core-shell triboelectric braided fibers and power textiles for energy harvesting and plantar pressure monitoring. *EcoMat*. 2022;e12191. doi:10.1002/eom2.12191